On the influence of temperature on the 1/2 screw dislocation core in uranium dioxide

Jules-Elémir Suchorski, Adrien Pivano, Jonathan Amodeo

Article published in Acta Materialia in 2025, please cite as :

Suchorski, Jules-Elémir, Adrien Pivano, and Jonathan Amodeo. "On the influence of temperature on the 1/2< 110> screw dislocation core in uranium dioxide." Acta Materialia (2025): 287, 120771.

On the influence of temperature on the 1/2<110> screw dislocation core in uranium dioxide

Jules-Elémir Suchorski[a], Adrien Pivano[a], Jonathan Amodeo[b]

[a] *CEA, DES, IRESNE, DEC, SESC, LM2C, Saint-Paul-Lez-Durance, F-13108, France*
[b] *Aix-Marseille Université, Université de Toulon, CNRS, IM2NP, Marseille, F-13013, France*

Abstract

Understanding the fundamental processes of plastic deformation in uranium dioxide (main nuclear fuel) is critical to predict the structural integrity of nuclear reactors under off-normal operating conditions. While the 1/2<110>{001} edge dislocation has been extensively studied in recent years due to its role as rate-limiting character for plastic deformation in the primary slip systems, much less is known about the screw dislocation, despite its recently shown involvement in the composite slip process at high temperature. Here, molecular simulations are employed to investigate the evolution of the 1/2<110> screw dislocation core structure in UO_2 with temperature. First, a comparison of the various interatomic models tested at 0 K addresses the stability of a *zig-zag* core structure predominantly spread in {001}. Then, molecular dynamics simulations confirm the stability of the screw dislocation core spread in {001} up to 1600 K, after which a transition towards more complex core structures involving the {110} and {111} planes is characterized, with direct implications on the shear-ability of the various crystallographic planes of the fluorite structure. Further analysis reveal that the transition of the screw dislocation core, that favors thermal fluctuation of the dislocation core in {111} slip planes at high temperature, is driven by the local disordering of the anionic sublattice within the dislocation core, preceding the well-known Bredig transition in UO_2. This transition of the screw dislocation core is at the roots of the composite slip process, which was recently proposed to explain the Schmid law breakdown observed in UO_2 single crystal.

Email address: jonathan.amodeo@cnrs.fr (Jonathan Amodeo)

Keywords: UO_2, screw dislocation, temperature, atomistic simulations, cross-slip

1. Introduction

Uranium dioxide (UO_2, fluorite structure) is the main fuel material used in nuclear power plants. During operation, UO_2 fuel pellets are subjected to extreme thermomechanical constrains with temperature variations ranging from *c.a.* 1200 K (nominal regime) to more than 2000 K (incidental to accidental regimes) at the pellet centerline [1, 2]. In particular, such behaviour can lead to a significant amount of creep stresses that can deform and damage both the fuel pellet and the surrounding metallic cladding tube. In this context, understanding the mechanical behaviour of nuclear fuels under the various conditions of operations *i.e.*, from nominal to incidental conditions, is of the utmost importance for nuclear safety [3, 4, 5].
As shown by mechanical testing and microscopy observations, 1/2<110>{001} slip systems (mode I) are the most prone to occur in UO_2 single crystal under compression [6, 7]. Additional observations confirm the activation of alternative 1/2<110>{110} (mode II) [8, 7] and 1/2<110>{111} (mode III) [9] slip systems where dislocation cross-slip is at the root of a composite slip hypothesis, especially at high-temperature [8, 10]. Beyond UO_2 single crystal brittle-to-ductile transition (*c.a.*, from ∼800 K) and up to 1700 K, critical resolved shear stresses (CRSS) are lower in {001} slip planes than in {110} and are particularly sensitive to temperature [11, 12, 6, 13, 8, 14, 15, 7, 9, 16, 17, 18]. Such a behaviour confirms that UO_2 is a material with high lattice friction with consequences upon the fine structure of dislocations and their mobility. Note that while few evidences of 1/2<110>{111} dislocations exist in UO_2, no CRSS measurement is available as mode III slip is always observed as a combination involving modes I and/or II. Due to lattice friction, dislocation microstructures observed in UO_2 below 2000 K using transmission electron microscopy (TEM) show dislocations with anisotropic shapes, extended edge segments and *zig-zag* portions in 1/2<110>{001} [6, 14, 7]. Thus, the glide of the 1/2<110> edge dislocation in {001} is known as the rate-limiting process in UO_2 single crystal and has led to several studies, especially relying on atomistic simulations [19, 17, 20, 21]. Also, the screw character was shown to be activated at larger stress than its edge counterparts for modes II and III at 0 K [22].

Despite these advancements, Portelette *et al.* have recently shown that the incipient plasticity of UO_2 single crystal could not be explained by the classical glide hypothesis, even if the latter incorporates all the slip systems of the fluorite structure [18, 23]. Indeed, Portelette's crystal plasticity approach partially failed at reproducing yield strengths and crystal rotations measured in the experiments of Sawbridge and Sykes [8] for various sample orientations, especially in cases of single mode deformation predictions. Finally, Madec *et al.* have shown that an hypothesis relying on the cross-slip of the screw dislocation might explain the aforementioned Schmid law breakdown in UO_2 single crystal using discrete dislocation dynamics (DDD) and CPFEM simulations [10]. In this study, the authors demonstrate that the orientation-dependent strengthening observed in the experiment can be reproduced when relying on favourable cross-slip conditions in the various slip modes of UO_2, bringing the 1/2<110> screw dislocation back at the heart of the debates while filling the gap between experiments and multi-scale models of UO_2 plastic deformation. Unfortunately, this hypothesis is quite qualitative and is limited by the lack of information about the dislocation structure and mobility at high-temperature, which can be generalized to most of other materials. Indeed, only a few studies conducted in BCC and HCP metals have focused on the sensitivity of the screw dislocation to temperature, highlighting the evolution of the core structure spread and its direct impact on the dislocation mobility, the latter depending on the slip system of interest [24, 25, 26, 27].

Up to now, the screw dislocation has been little studied in UO_2, probably due the predominance of the 1/2<110>{001} slip system which is known to be constrained by the low mobility of the edge dislocation [19, 28, 22, 29, 30]. Still, Soulié and collaborators used atomistic simulations and the variable charge second-moment tight-binding QEq (SMTB-Q) interatomic potentials to model both the 1/2<110> screw and edge {001} dislocation cores. In particular, the authors identified a stable configuration for the screw dislocation core with a centred column of oxygen atoms that alternates along the dislocation line, in a similar fashion that what is observed for the {001} edge *zig-zag* dislocation core [30, 21]. Also, Lunev *et al.* [29] have investigated the thermally-activated glide of the screw dislocation in the {110} slip plane using atomistic simulations. Among others, the authors underline the complexity of the various glide processes including kink-pair nucleation/propagation, dislocation self-pinning or splitting out of the glide plane, point defects

and Frank loops emission from the dislocation, but do not address neither the dislocation core structure nor cross-slip in the various slip modes.
In this study, atomistic simulations are used to investigate the 1/2<110> screw dislocation core with an original emphasis on the influence of temperature on the dislocation core spread that helps to better contextualise dislocation glide and cross-slip in UO_2 at elevated temperature.

2. Methods

Atomistic simulations are performed using the LAMMPS code [31] and three various interatomic potentials, namely the Cooper, Rushton and Grimes (CRG), the MOX-07 and the SMTB-Q [32, 33, 34], used to model the interactions between atoms in UO_2. The CRG potential combines pair and embedded atom method (EAM) [35] interaction terms and is renown for its ability to model UO_2 single crystal thermomechanical properties including *e.g.*, lattice parameters, anisotropic elasticity, stacking-fault energies (SFE), dislocations and grain boundaries [32, 20, 36, 37, 38]. The MOX-07 potential is derived from the rigid ion pair model and is now commonly used to model thermo-mechanical studies of UO_2. Recently, MOX-07 was successfully used to model dislocation core and mobility [20, 29, 21, 39]. However, it is known to poorly describe UO_2 elastic constants when compared to DFT calculations and experiments [36, 38]. Here, the CRG and MOX-07 potential rely both on a 11 Å short-range interaction cutoff. The SMTB-Q potential is the more sophisticated approach used in this study as relying on variable charge equilibration based on the Qeq approach [40, 41, 42]. It has shown to be one of the finest interatomic potential to model lattice, phase stability, oxygen migration, SFE and dislocation properties in UO_2, especially at 0 K when compared to DFT simulations [30, 34, 21]. Nevertheless, this high-precision is obtained at the cost of high cpu costs that preclude large-scale molecular dynamics (MD) simulations. Thus, SMTB-Q will be used here for comparison purpose only, especially at 0 K. Both the particle-particle particle-mesh (PPPM) [43] and Wolf [44] charge summation methods are employed depending on the simulation boundary conditions (BCs) and the interatomic potential used. On the one hand, the Wolf truncation is used when relying on semi-periodic BCs with a radius of 11 Å and a damping coefficient of 0.3 $Å^{-1}$ for the three interatomic potentials. On the other hand, the PPPM method with a relative error of 10^{-5} is used when relying on 3D periodic

boundary conditions (3D-PBCs) for CRG and MOX-07 both used with a 11 Å long-range cutoff, while SMTB-Q relies exclusively on the Wolf method due to compatibility, using the same parameters as mentioned above. In addition to prior observations [21], no quantitative differences were noticed here when comparing results obtained from both charge summation methods (more details in the following).

The screw dislocation core structure at 0 K is investigated using the dislocation dipole method with 3D-PBCs as shown in Figure 1a. First, a fluorite UO_2 simulation cell of dimensions L_x=239.0 Å, L_y=15.4 Å (dislocation length l=4b) and L_z=239.9 Å (with slight variations depending on the interatomic model used), oriented along $x = [1\bar{1}0]$, $y = [110]$ and $z = [001]$, is designed using ATOMSK [45]. Then, a screw dislocation dipole with opposite Burgers vectors $\vec{b}$=$\pm$1/2[110]a_0 is introduced (quadrupolar configuration [46]) using the isotropic linear elasticity with Burgers vectors and dislocation lines aligned along the y-direction. This setup allows for a rigorous evaluation of the dislocation elastic energy and is preferred while computing stable dislocation core structure [47, 48]. In particular, the quadrupolar screw configuration preserves both the 3D-PBCs and the neutral net charge of the whole simulation box. Note that simulation box dimensions are chosen in line with previous studies performed on dislocation modeling and size-effects in UO_2 relying on the same dipolar method [21, 39].
After sample design, the dislocation dipole is relaxed using the conjugate gradient (CG) method with box relaxation (zero stress targeted for each term of the stress tensor using a triclinic-cell) and the FIRE algorithm (with fixed box) [49], consecutively. Among others, this relaxation procedure allows to accommodate the plastic shear induced by the dislocation dipole. During the simulation, a force tolerance on the atoms of at least 10^{-4} eV/Å is used as a convergence criterion for the three interatomic potentials tested. Please note that the same criterion is used for all energy minimization simulations later presented in this study. After energy minimization, the dislocation core energy at 0 K $E_{core}(r_c)$ is computed in a stoichiometric compound using Equation 1,

$$E_{tot} = NE_0 + E_{elastic}(r_c) + 2E_{core}(r_c) \quad (1)$$

with E_{tot} the potential energy of the system, N the number of UO_2 molecules, E_0 the energy per-molecule computed in the perfect crystal and $E_{elastic}(r_c)$

the elastic energy computed using the Babel software [50] over the whole simulation cell, excluding cylinders of radius r_c centered around each dislocation. r_c=2b is chosen here, consistent with the work of Soulié *et al.* [30]. Note that two types of 0 K configurations are discussed in the following: $E_{core}^{0K}(r_c)$ is obtained minimizing the energy of the the as-prepared sample following the aforementioned procedure (classical approach), while $E_{core}^{h/q}(r_c)$ is computed using a specific MD heating/quenching cycle and the same energy minimization routine (more details in the following). All along the study, the local crystal structure and dislocation analysis are performed using the Polyhedral Template Matching (PTM) algorithm as implemented in OVITO [51, 52], applied to the uranium atoms sublattice with a RMSD cutoff of 0.15. In addition, dislocation core structures are analyzed using differential displacement maps computed from dislocation slices of thickness b with Atomman [53] and disregistry profiles $\phi_i(x_i)$ using a homemade routine and adjusted as follows,

$$\phi_i(x_i) = \frac{b}{\pi} \arctan \frac{x_i}{\zeta_i} + \frac{b}{2} \tag{2}$$

where x_i is the atom coordinate in the i plane and ζ_i a fitting parameter which characterizes the half-width of the dislocation core in plane i.

The influence of temperature on the dislocation core spread is studied using the semi-periodic BCs method where the simulation cell contains a single dislocation [54, 55, 56]. This method is preferred here to avoid dislocation dipole annihilation promoted by temperature-induced cross-slip events. Also, it is worth to notice that the modelling of a single dislocation prevents the use of 3D-PBCs and leads to polarized surfaces. Here, an extended simulation cell of dimensions L_x=300.7 Å, L_y=15.4 Å (4b) and L_z=299.8 Å is designed (same orientation than previous case). After simulation cell design, the sole 1/2<110> screw dislocation is introduced in the mid of the xz plane using the isotropic elasticity theory. Consequently, PBCs are maintained in the xy plane while fixed BCs (FBCs) are set along the z direction (Figure 1b). Also, the simulation cell y-vector is tilted along x by δx=b/2 to both accommodate the plastic shear induced by the dislocation and recover periodicity along the x direction. Afterwards, the system energy is minimized using an iterative process made of CG minimization (using constant cell dimensions) and consecutive cell vectors adjustments, the later allowing pressure relaxation along the three cell directions (same method than in ref. [29]). Finally, the FIRE

algorithm (using constant cell dimensions) is used to complete the energy minimization process once the minimum stress is reached. Note that for the single dislocation protocol, a layer of atoms of 13 Å thick at z boundaries is frozen in the z-direction during the whole simulation process to avoid spurious surface effects.
Heating using MD and the CRG potential is performed within the NVT ensemble using the Nosé-Hoover thermostat [57]. Note that an integration timestep of 1 fs is used in all MD simulations in the study. For each temperature of interest, the simulation cell is first expanded using a second order polynomial adjustment of the lattice parameter a_0 variations with temperature ($\Delta a_0/a_0$=1.002 + 4.975 $\times 10^{-6} \times T$ + 3.205 $\times 10^{-9} \times T^2$) [32], then the sample is heated at a maximum heating rate of 50 K.ps^{-1} up to the target temperature at which a final pressure equilibration run is performed, adjusting box dimensions. Temperature-dependent disregistry profiles and differential displacement maps are computed on partially quenched (20 CG steps) configurations [58, 26]. For statistical considerations, these configurations are generated every 100 MD steps. Note that the few MD simulations performed on the quadrupolar configuration to compute $E_{core}^{h/q}(r_c)$ are performed in the NPT ensemble maintaining zero pressure. Additional simulations with a dislocation length l=24b have been conducted for comparison when necessary.

3. Results and discussion

3.1. 1/2<110> screw dislocation core at 0 K : stable vs. metastable configurations

The relaxed configuration of the 1/2<110> screw dislocation core at 0K is shown in Figure 2a-c. Results reveal the same characteristic configuration (waviness of oxygen columns in the (001) plane) for the three interatomic potentials tested, similar to what observed by Soulié *et al.* using the SMTB-Q potential [30]. The dislocation core energy $E_{core}^{0K}(2b)$ is 1.422, 1.538 and 1.180 eV/Å for the SMTB-Q, CRG and MOX-07 potentials, respectively (see Table 1). Nevertheless, this core structure is not stable while heating. Indeed, when heated up to 300 K and quenched back to athermal conditions minimizing the energy of the system, the relaxed configuration obtained with CRG or SMTB-Q is 2b-periodic and characterized by the splitting of oxygen columns in the core (*zig-zag* configuration) as shown in Figure 2d,e. Additional details regarding the periodicity of the dislocation core along the dislocation

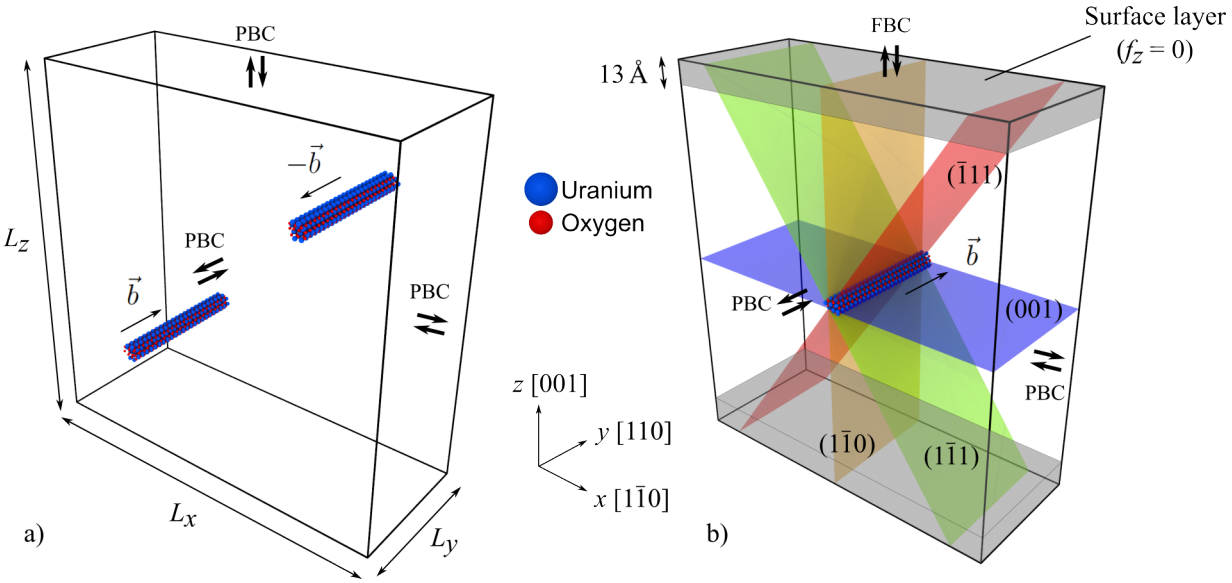

Figure 1: Screw dislocation core modeling protocol using a) a dipole setup with 3D-PBCs for 0 K dislocation core study and b) a semi-periodic setup (FBCs used along z, PBCs elsewhere) to investigate the influence of temperature. Perfect crystal atoms are removed for the sake of clarity.

line are provided in the supplementary information. This oxygen reorganization deep in the dislocation core results in a diminution of the core energy of about -0.1 eV/Å when comparing $E_{core}^{h/q}(2b)$ to $E_{core}^{0K}(2b)$ (Table 1), which emphasizes the better stability of the *zig-zag* core for the two potentials. It is worth noticing that a similar *zig-zag* configuration was already discussed by Soulié *et al.* using the SMTB-Q potential resulting in comparable core energy (less than 5% variation), despite the slight methodological differences [30]. Moreover, the *zig-zag* arrangement of oxygen atoms induced by temperature is also discussed in the case of the 1/2<110>{001} edge dislocation, modeled using SMTB-Q, MOX-07 and DFT [21], confirming the propensity of oxygen atoms to alternate positions in a *zig-zag* way along the dislocation line in UO_2.

However, it is noteworthy that the misalignment of oxygen atoms is less pronounced for the MOX-07 potential than for SMTB-Q and CRG, even when heating up to T =1000 K (while a few tens of K already show the transition for the two other potentials). Furthermore, applying the heating/quenching method to MOX-07 does not lead to a significant variation of the core en-

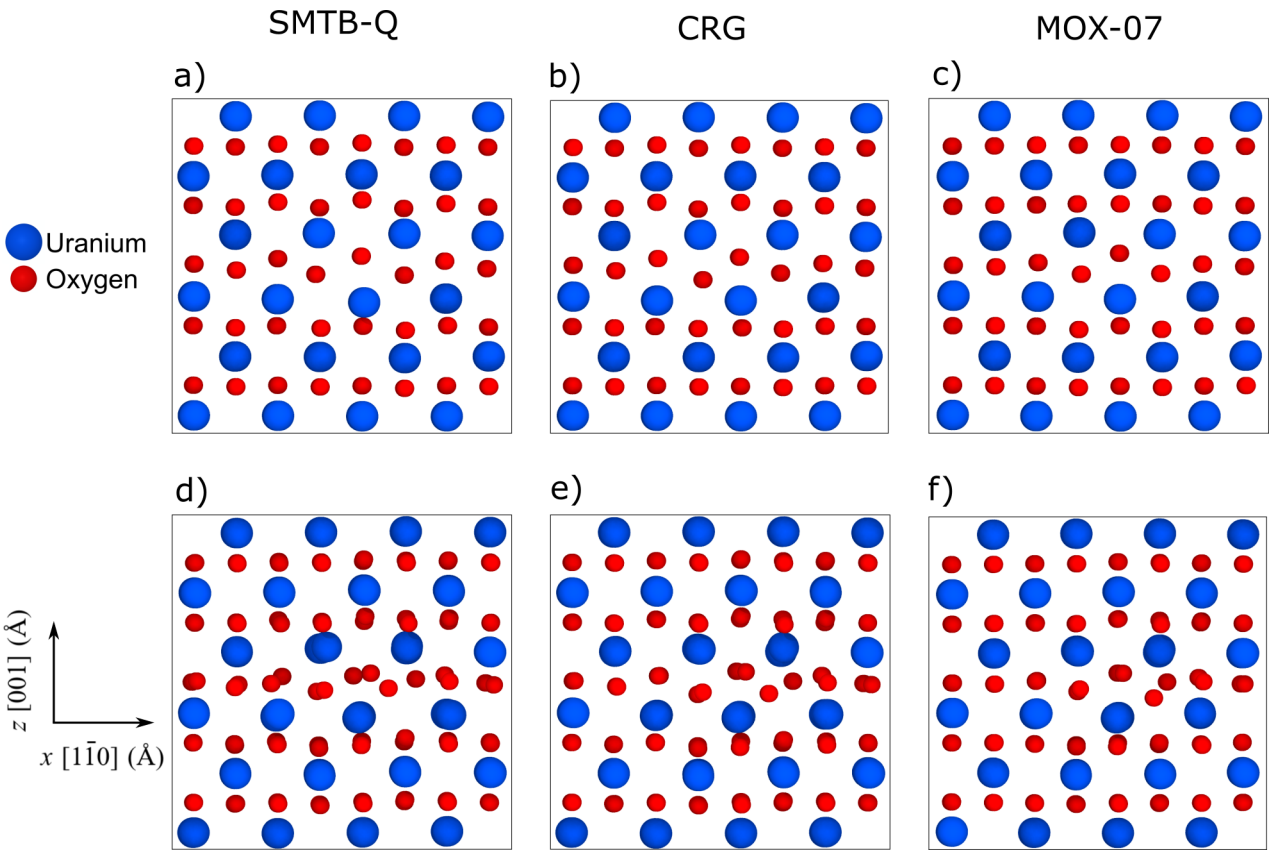

Figure 2: 1/2<110> screw dislocation core computed at 0 K using the a,d) SMTB-Q, b,e) CRG and c,f) MOX-07 interatomic potentials. a-c) Configurations obtained after classical 0 K energy minimization, d-e) configurations obtained using the heating/quenching method with a maximum temperature of 300 K, f) configuration obtained after energy minimization using the MOX-07 potential with the SMTB-Q (d) or CRG (e) relaxed configuration as an input.

Table 1: 1/2<110> screw dislocation core energy in UO_2 computed at 0 K (E_{core}^{0K}) and after the heating/quenching cycle ($E_{core}^{h/q}$) using Equation 1 and r_c=2b.

Energy (eV/Å)	SMTB-Q	CRG	MOX-07
E_{core}^{0K}	1.422	1.538	1.180
$E_{core}^{h/q}$	1.322	1.426	1.180±0.005

ergy *c.a.*, $E_{core}^{0K}(2b) = 1.180$ and $E_{core}^{h/q}(2b) = 1.180 \pm 0.005$ eV/Å, respectively, $E_{core}^{h/q}(2b)$ depending only on the details of the high-temperature configuration to be quenched *i.e.* with more or fewer oxygen atoms in alternating positions. To further evaluate the ability of MOX-07 to stabilize the *zig-zag* core, the *zig-zag* configurations obtained with the SMTB-Q and CRG (Figure 2d,e) were both used as input for additional energy minimization simulations using the MOX-07 potential. Both simulations lead to the exact same *zig-zag* configuration shown in Figure 2f (comparable to those obtained using CRG or SMTB-Q) and characterized by $E_{core}^{h/q}(2b) = 1.182$ eV/Å. Reproducing MOX-07 simulations with an increased dislocation length ($l = 24b$) and a maximum heating temperature of 1000 K shows partial alternation of oxygen atoms in the core, without significant impact on $E_{core}^{h/q}(2b)$. Overall, these results confirm the stability of a *zig-zag* core configuration for the 1/2<110> screw dislocation in UO_2, which levels the dislocation core energy by breaking the symmetry of the oxygen atoms alignment.

Figure 3 shows the differential displacement maps of uranium atoms for the *zig-zag* screw dislocation core computed at 0K (*i.e.*, corresponding to configurations of Figure 2d-f). For the three interatomic potentials, the dislocation core location (identified at the centre of the most extended arrow) is in the middle of a parallelogram, made of four columns of atoms tilted either to the right or to the left, both configurations being equivalent due to crystal symmetries. Overall, differential displacement maps show that the 1/2<110> screw dislocation core is more spread in the (001) plane, especially when relying on SMTB-Q and CRG, while MOX-07 is characterized by a configuration a little more symmetric. This property is further investigated computing disregistry profiles ϕ_i (Equation (2)) in the main crystallographic planes *i.e.* (001), $(1\bar{1}0)$ and the two $(\bar{1}11)$ and $(1\bar{1}1)$ planes while $\vec{b}$=1/2[110] (Figure 4). Note that computed differential displacement maps and disregistry profiles (both computed on 1b dislocation slices) do not vary significantly

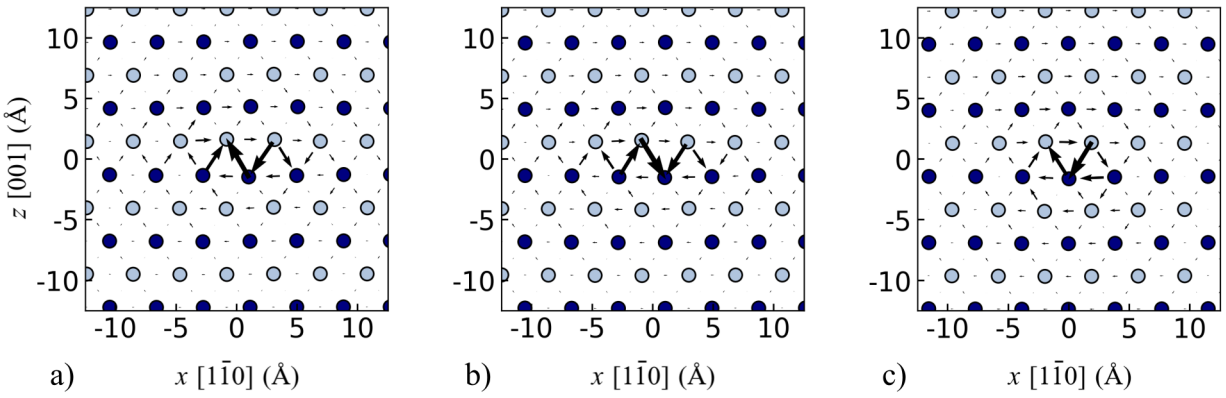

Figure 3: Differential displacement maps for the 1/2<110> screw dislocation in UO_2 computed at 0 K (heating/quenching method) using the a) SMTB-Q, b) CRG and c) MOX-07 potentials. Light- and dark-blue atoms belong to two different (110) planes. Black arrows characterize the differential displacement of the atoms when compared to the perfect crystal configuration. The size of the arrow scales with the amplitude of the atomic displacement along the $y = [110]$ direction. For the sake of clarity, the displacement maps are computed for the U sublattice only.

Table 2: Dislocation core half-width ζ_i^{0K} (Å) computed in {001}, {110} and {111} at 0 K (CRG potential). Results are averaged along the dislocation line.

i plane / Potential	(001)	(1$\bar{1}$0)	($\bar{1}$11)	(1$\bar{1}$1)
SMTB-Q	2.7	1.2	1.3	1.2
CRG	2.7	1.2	1.2	1.2
MOX-07	1.8	1.3	1.5	1.7

along the dislocation line, as relying on the uranium sublattice only. Also, fitting the disregistry confirms the extension of the screw dislocation core in {001} at 0 K, especially for CRG and SMTB-Q that show the same maximum values of the dislocation core half-width in (001), $\zeta_{(001)}^{0K}$ ∼2.7 Å, while ζ_i^{0K} is about 1.2-1.3 Å only, for the three other crystallographic planes (see Table 2). ζ_i^{0K} values obtained for MOX-07 confirms the more symmetrical spread of the dislocation core for this latter parameterization.

While the SMTB-Q formalism has shown in the past to be particularly transferable to dislocation core simulation in UO_2 [21], here we show that

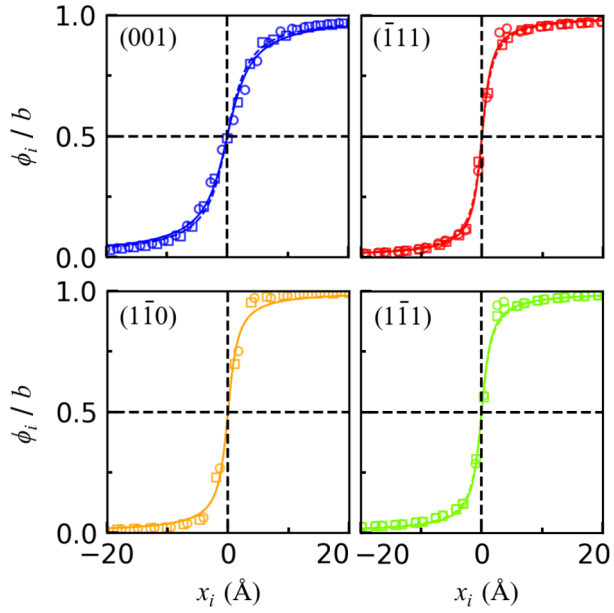

Figure 4: Disregistry profiles for the 1/2<110> screw dislocation *zig-zag* core computed at 0 K using the CRG potential in (001), ($\bar{1}$10), (1$\bar{1}$0) and (11$\bar{1}$). Symbols and curves correspond to explicit calculations and fit (Equation (2)), respectively. Squares and circles (dashed and solid lines, respectively) rely on calculations performed on two consecutive slices of thickness b, along the dislocation line.

the CRG potential leads to comparable results for the 1/2<110> screw dislocation, both in terms of dislocation core atomic configuration and energy. Also, the more symmetrical core observed with MOX-07 may be attributed to inaccuracies in the interatomic potential regarding the elastic constants [36]. Bearing these aspects in mind along with the high cpu costs associated with SMTB-Q, the rest of the study will rely on the CRG potential only.

3.2. Influence of temperature on the 1/2<110> screw dislocation core

In the following, the 1/2<110> screw dislocation core is investigated at high temperature using MD simulations with semi-periodic BCs conducted at constant temperature (CRG potential, Wolf method, NVT ensemble), with no applied stress. Here, temperatures up to to 2200 K (typical of the nuclear transient) are investigated during 2 to 4 ns. Please note that changing the charge summation method here (when compared to simulations presented in Section 3.1) did not impact the low-temperature dislocation core structure. For each MD simulation, atomic positions are recorded every 100 fs and instantaneous disregistry profiles and ζ_i are computed (see section 2 for more technical details). Note that spurious data that could not be accurately adjusted using Equation (2) due to thermal noise were removed from the rest of the analysis.

The detailed statistical distributions of the dislocation core half-width $P(\zeta_i)$ are illustrated in Figure 5. At T=1400 K, $P(\zeta_{(001)})$ is centered around $\zeta_{(001)}$=2.8 Å, particularly close to the value obtained at 0 K (*i.e.*, 2.7 Å), which might suggest that the core topology is stable over the entire 0-1400 K temperature range. The dislocation core spread in (001) at 1400 K is also confirmed by the calculation of instant differential displacement maps (Figure 6a,b). However, $P(\zeta_{(001)})$ shifts towards lower values of $\zeta_{(001)}$ when temperature increases while the other distributions, and especially both $P(\zeta_{\{111\}})$, show the opposite trend. An abrupt transition occurs between 1600 and 1800 K where the two $P(\zeta_{\{111\}})$ change from a sharp distribution centered on 1.2 Å (again, close to the 0 K values) to a broader one shifted towards larger ζ_i values. This tendency is illustrated in Figure 6c-f where more diversified core structures are identified from the instant differential displacement maps computed at T=2000 K with core configurations that (i) either spread in each of the two {111} planes (*e.g.*, Figure 6c,d), (ii) exhibit narrower structures (Figure 6e) or (iii) show even more complex atomic arrangements influenced

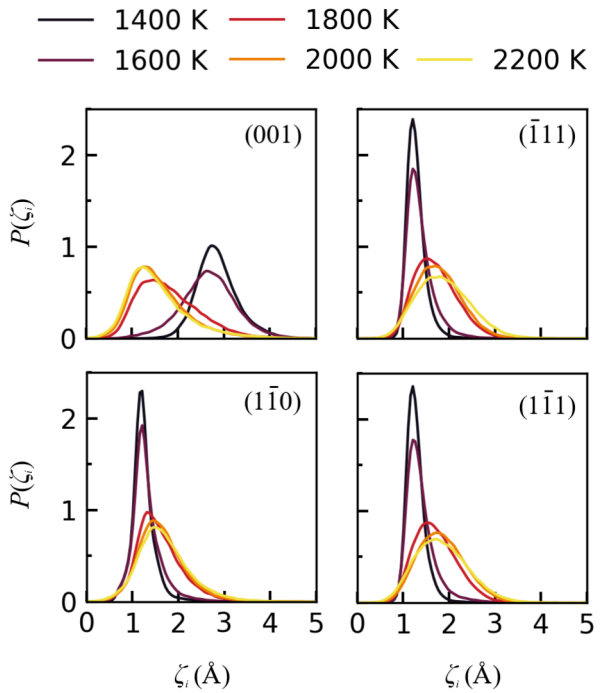

Figure 5: Distribution of instant dislocation core half-width in the main crystallographic planes $P(\zeta_i)$ for the 1/2<110> screw dislocation computed during MD simulation at various temperatures (measure every 100 fs, CRG potential).

by thermal noise (Figure 6f). The evolution of the mean of the dislocation core half-width $<\zeta_i>$ as a function of temperature is illustrated in Figure 7 where the transition from a core spread in (001) at low-T towards more complex core configurations at temperatures beyond 1600 K is confirmed.

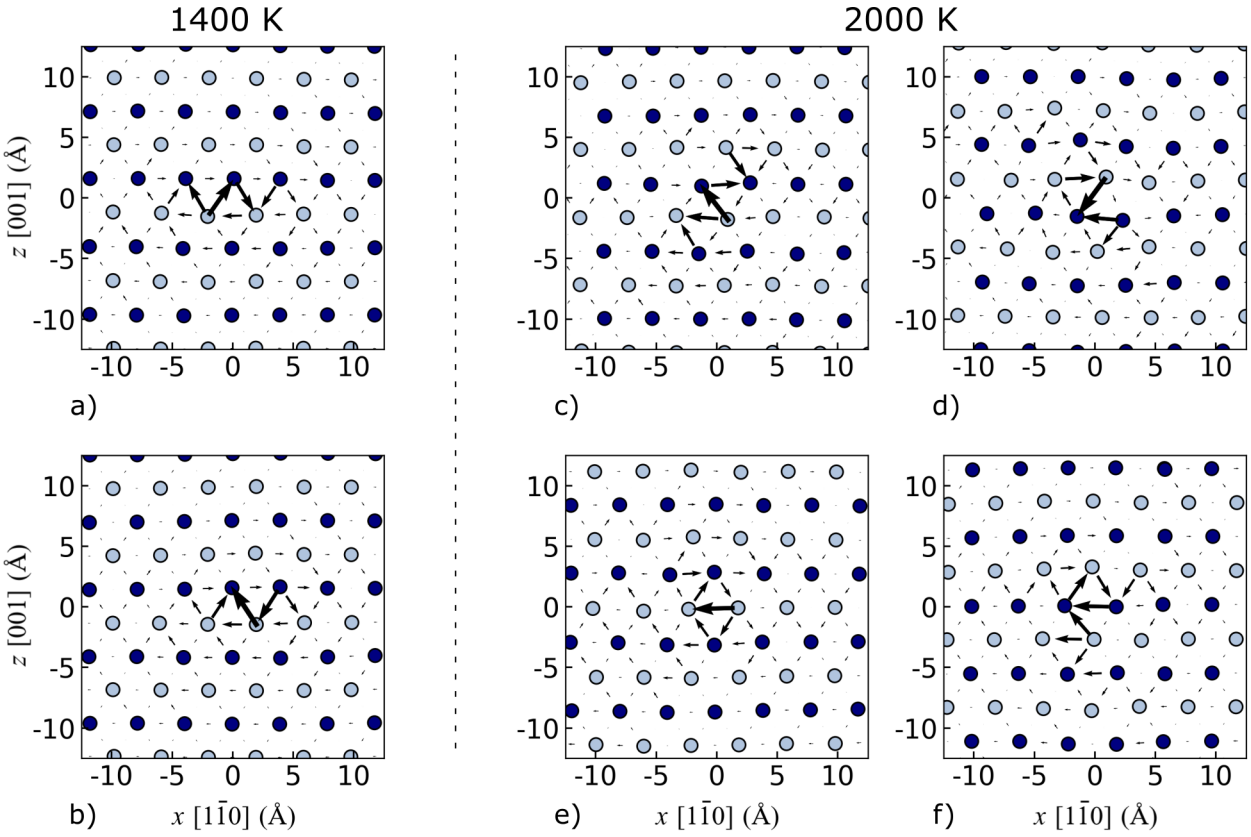

Figure 6: Instantaneous differential displacement map of the screw dislocation core computed during MD simulation at a) 1400 K and b) 2000 K. Simulations are performed using the CRG interatomic potential.

MD simulations performed at constant temperature are characterized by the fluctuations of the mean position of the dislocation core (Figure 8). To further investigate the relation between the dislocation core spread and the various slip planes, we categorized dislocation core configurations along time by classifying ζ_i instant values *i.e.*, if ζ_i exceeds all other ζ_j by a certain fraction f, then the core is considered to be spread in plane i. Conversely, the core

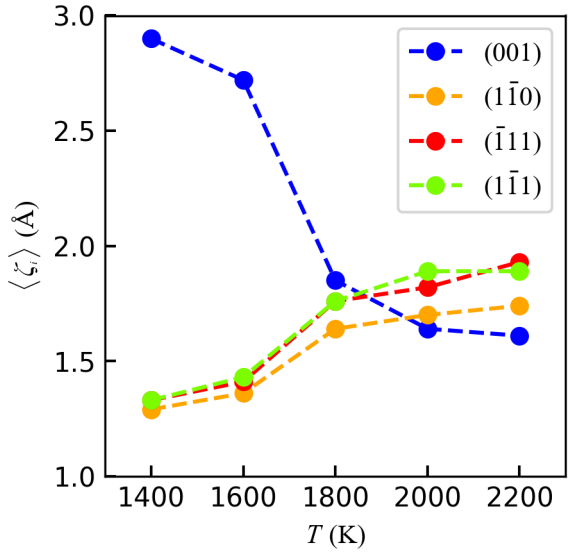

Figure 7: Evolution of the mean dislocation core half-width per plane $<\zeta_i>$ computed during NVT MD simulation (CRG potential) as a function of temperature.

is classified as *symmetric* (*i.e.*, without preferential habit plane) if none of the planes meet this condition. Results obtained for $f = 10\%$ are illustrated in Figure 8 (a parametric study varying f is provided in the supplementary information). Overall, the dislocation core position mostly fluctuates in the same (001) plane at 1400 K under the sole effect of temperature, with only occasional stays in adjacent (001) planes allowed by cross-slip through (1$\bar{1}$0). It is worth mentioning that (1$\bar{1}$0)-core configurations are identified here only during cross-slip while glide in (001) is mostly associated to (001) core configurations. At 1600 K, fluctuations in (001) are still predominant. Also, while cross-slip in (1$\bar{1}$0) is still observable, one can notice more cross-slip events in the ($\bar{1}$11) and (1$\bar{1}$1) planes, with according core spread. The dislocation ends up fluctuating mostly in the two {111} planes increasing the temperature to 1800 K and further *i.e.*, without anymore glide or cross-slip events in (001) nor (1$\bar{1}$0). This result is illustrated by the dislocation trajectory analysis that shows a majority of {111}-extended core configurations for $T \geq 1800$ K. In contrast, minor {110} slip events appear to be constrained to the $T \leq 1800$ K range, where they occur less frequently than {001} slip events. Finally, one can note that symmetric core configurations are quite homogeneously

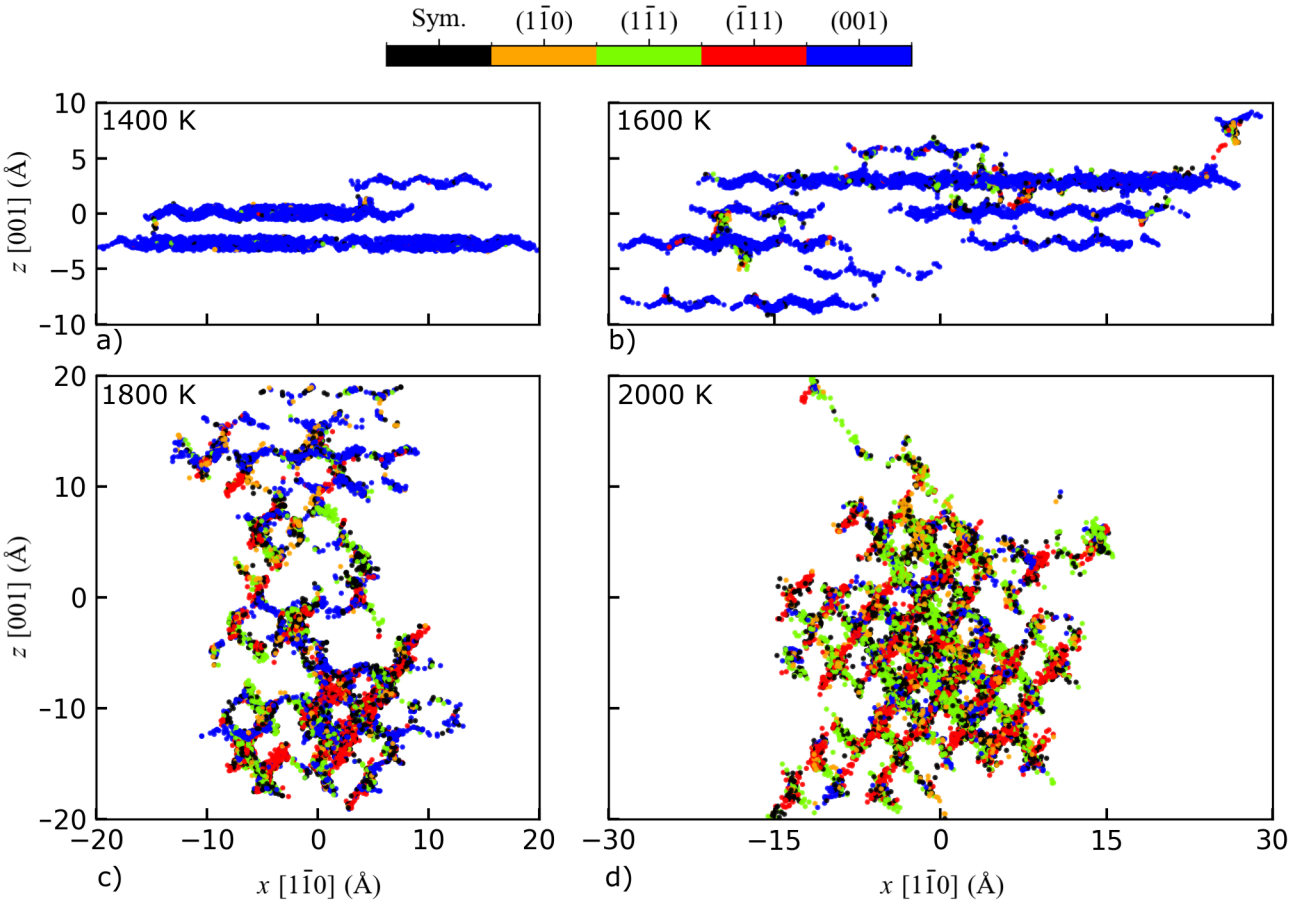

Figure 8: Dislocation core position fluctuations during MD simulations (NVT, zero stress) performed at a) 1400 K, b) 1600 K, c) 1800 K and d) 2000 K. Simulations are performed using the CRG interatomic potential.

distributed between the various slip planes *i.e.*, they are not associated with slip or cross-slip in any particular plane, and their ratio increases from 2% to 27% (for $f = 10\%$) increasing the temperature from 1400 to 2000 K.

4. Discussion

The investigation of nuclear fuel mechanical integrity is crucial in the context of nuclear safety, especially in the off-normal conditions of operations that cover temperatures from 1400 K to melting temperature. In this context, several recent modeling studies have focused on gaining a better understanding of the elementary deformation processes responsible for the irreversible deformation of UO_2 at the grain scale. Concerning dislocations, a significant piece of work was conducted on the 1/2<110>{001} edge dislocation that is known to be the rate-limiting character for the primary 1/2<110>{001} slip systems (see *e.g.*, [17, 20, 30, 21, 39]). In particular, Fossati *et al.* have computed the 1/2<110>{001} edge dislocation core structure and the CRSS in the 3 modes of deformation of UO_2 using MD. Also, Soulié and collaborators have recently investigated dislocation core structure in UO_2 using SMTB-Q and molecular static simulations. While the authors carefully detailed the 1/2<110>{001} edge dislocation core and mobility based on Peierls stress and kink-pair calculations, only few information are provided on the screw dislocation core and the sensitivity of its slip ability regarding temperature is not addressed. In this context, Lunev and collaborators have investigated the 1/2<110> screw dislocation mobility in {110} (deformation mode II), relying exclusively on the MOX-07 interatomic potential [29]. In this study, the motion of the screw dislocations is found to be influenced by several thermally-activated processes (partial dissociation, self-pinning and unpinning processes, defect emission, *etc.*), but no explicit correlation is made with the dislocation core or its temperature dependence.
Still, the role of the screw dislocation upon the deformation of UO_2 was mentioned already in the early 70s within the work of Sawbridge and Sykes [8]. In this study, the authors emphasized the breakdown of the Schmid-law when applied to UO_2 single crystal compressed at T=1600 K and attributed it to the possible activation of modes II and III dislocations. In particular, the authors mentioned cross-slip with macroscopic (and somehow wavy) {110} and crystallographic {111} slip traces, supporting the hypothesis of a composite slip mechanism (*i.e.*, multi-slip mode plastic deformation), more prone to operate due to the unique type of Burgers vector shared between

the three slip modes (each Burgers vector is shared between four of the slip systems). While dislocation cross-slip was recently observed using TEM in polycristalline UO_2 deformed at high temperature [59], the composite-slip hypothesis was only recently revisited in UO_2 using a multi-scale modeling approach relying on discrete dislocation dynamics and crystal plasticity finite-element simulations [10]. In Madec *et al.*, the authors have shown that an assumption based on a particularly-effective cross-slip between parts of the slip systems (*i.e.*, cross-slip with a low-activation stress) was able to justify the Schmid-law breakdown observed by Sawbridge and Sykes. Indeed, the authors highlight the increase of the computed critical resolved shear stress (closer to experimental values) when cross-slip was turned on, especially for orientations where the Schmid law does not apply. Nevertheless, this study suffers from a quantitative parameterization of the cross-slip process that remains mostly phenomenological.

In our study, the sensitivity of the 1/2<110> screw dislocation core to temperature is investigated using atomistic simulations relying on some of the best interatomic potentials currently available in the literature. At 0 K, simulation results show that the screw dislocation mostly spreads in the {001} slip plane. Also, the more stable dislocation core configuration was characterized by the split of oxygen atomic columns in a *zig-zag* way, in a similar manner that what was observed for the 1/2<110>{001} edge dislocation [21]. However, the screw dislocation core topology becomes increasingly complex with rising temperature. Indeed, while instantaneous differential displacement maps show immediate variations in the dislocation core induced by temperature, trajectories obtained from MD fluctuation simulations confirm the evolution of the shear-ability of the various crystallographic planes. Specifically, the temperature-induced fluctuations of the dislocation core occur almost exclusively in {001} up to 1600-1800 K, beyond which they are replaced by fluctuations in {111}, initially via stochastic cross-slip events and subsequently through nearly exclusive dislocation glide in {111}. It is worth noticing at this stage that, although strong correlations were observed between the dislocation core half-width ζ_i and the favorable slip plane observed during MD fluctuation simulations, the increase of $\zeta_{(110)}$ configurations with temperature did not translate into more frequent slip events in {110}. Still, these results are another proof of the screw dislocation propensity to pass from a deformation mode to another in UO_2 when the temperature is large enough *i.e.*, over ∼1600-1800 K temperature, even without applied stress.

While these results align with the aforementioned experimental or modeling cross-slip hypothesis, further investigations are conducted in the following to identify the physical origins of such a behavior. In particular, the behavior of the oxygen atoms sublattice caught our attention. Figure 9a-d show the evolution with temperature of the screw dislocation core structure from an other perspective *i.e.*, including both the uranium and oxygen sublattices. In particular, we observed that the oxygen sublattice significantly disorganizes nearby the dislocation core beyond a certain temperature, while remaining fully ordered in the rest of the simulation cell. On the other hand, the uranium is only poorly impacted by the temperature variations in the range under investigation.

To quantify this aspect, the PTM method is used to compute the fraction of oxygen atoms in defective positions $O_{def} = N_{O_{def}}/N_O$ with $N_{O_{def}}$ and N_O respectively the number of oxygen atoms out of their original cubic lattice and the total number of O atoms (Figure 9e). The analysis is performed within a cylinder of radius 20 Å around the dislocation centre , as well as in the perfect crystal for comparison. At low temperatures, O_{def} increases slowly and linearly in the dislocation core region when raising the temperature (dO_{def}/dT=5.7 10^{-6} K^{-1}) up to a critical temperature T_c=1600 K, where O_{def} abruptly increases. For $T > T_c$, O_{def} increases with a rate of about 2.0 10^{-4} K^{-1}, about 35 times faster than below T_c, as a signature of the oxygen sublattice destabilization nearby the screw dislocation. Note that in the absence of dislocation, dO_{def}/dT increases more steadily without sign of abrupt transition up to the Bredig transition [60, 61, 62, 63, 64, 65, 66, 67, 68, 69], nearby 2700 K. The Bredig transition is a well-known phenomenon in fluorite bulk crystals, associated with the disordering of the anionic sublattice, occurring at approximately $0.8 \times T_m$ (where $T_m \sim$3100 K is the melting temperature). This property was observed before in UO_2 laser flash experiments [60, 61, 62] at temperatures close to 2700 K, as well as in other fluorite materials [63, 64, 65]. Similar observations were also made using MD simulations (see *e.g.*, [66, 67, 68, 69]). However, a complete consensus has not yet been reached for UO_2, owing to the challenges in obtaining precise measurements at high temperature. Figure 9 confirms that the ordering of the anionic sublattice shows an anticipated Bredig transition nearby the screw dislocation core at T_c=1600 K. It is worth mentioning that this critical temperature coincides exactly with the temperature at which the screw core starts swapping from {001} to more complex core spreading that involve also {110} and {111} (Figure 6 and 7), which results in more and more fluctuations in the

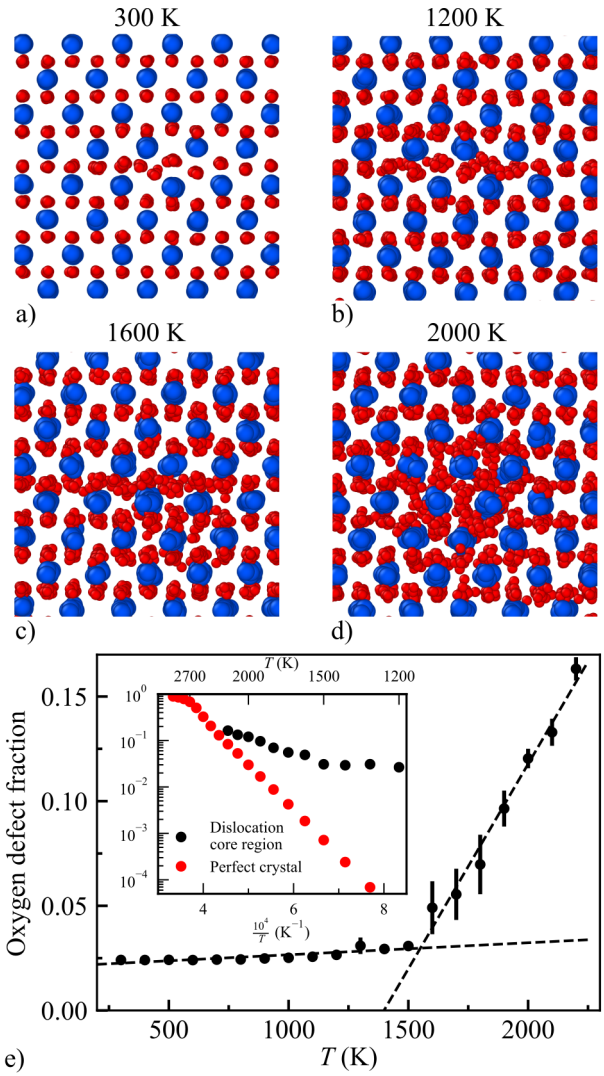

Figure 9: Evolution of the atomic disordering in the vicinity of the screw dislocation core as a function of temperature, a) 300 K, b) 1200 K, c) 1600 K, d) 2000 K, e) fraction of oxygen atoms in defective position (O_{def}) as function of temperature. An arrhenius plot is shown in the inset for comparison with the crystal without dislocation. Simulations are performed using the CRG potential.

{111} slip planes (Figure 8).
The challenging activation of {001}, {110} and {111} slips with temperature in UO_2 is often discussed in terms of lattice friction and electrostatic interactions. While the electrostatic screening resulting from the alternation of cationic/anionic crystallographic planes justifies the softer activation of the 1/2<110>{001} slip systems, the reverse reasoning is commonly invoked to explain the more difficult activation of 1/2<110>{111} in fluorite materials at low temperature (see *e.g.*, ref.[8]). Thus, we believe that both effects are compromised when the oxygen sublattice undergoes deorganization *i.e.*, the screening effect becomes less effective due to the loss of symmetry which increases the friction force in 1/2<110>{001} while decreasing it in the other slip modes, ultimately making all slip planes electrostatically more equivalent. Here, the deorganization of the oxygen sublattice is interpreted as a local phase transition, where UO_2 shifts from the fluorite structure (with screw dislocation core spread in {001}, and strong electrostatic frictions in {111} and {110}) to a more "metallic-like" configuration, characterized by a face-centered cubic (FCC) uranium sublattice immersed in a sea of oxygen atoms. In this configuration, electrostatic interactions play a less critical role in slip system activation, which relies on more complex screw dislocation core configurations that promote glide in {111}, the dense planes of the FCC structure. Thus, we believe that the local deorganization of the oxygen sublattice in the dislocation core is the main effect responsible for the screw dislocation core spread and the shear-ability properties observed in UO_2 increasing the temperature beyond 1600 K.

5. Conclusion

Dislocation modeling is of prime importance for nuclear fuel materials in order to improve predictive models of mechanical integrity developed in the context of nuclear safety. While the edge 1/2<110>{001} dislocation has attracted a significant attention in the recent years, here we focus on modeling of the 1/2<110> screw dislocation implicated in the composite slip process (via cross-slip), one of the main plastic deformation process at 1600 K and beyond. Upon the detailed description of the dislocation core nature, here we have shown that temperature has a significant impact on the fine structure of the core with a stable configuration at 0 K characterized by *zig-zag* oxygen atoms only observable after prior heating using MD simulation. Also, the

screw dislocation core that originally mostly spreads in {001} at low temperature shows more complex configurations that involve {110} and {111}, for temperature larger than 1600 K. MD fluctuation simulations performed at zero stress undoubtedly emphasize the ability of the screw dislocation core to move within {111} crystallographic planes while the temperature increases while, simultaneously, the oxygen sublattice of UO_2 progressively deorganizes. As a consequence, we believe that the screw dislocation core evolution and, more broadly, the cross-slip in {111} of the screw dislocation, are related to a local and anticipated Bredig transition nearby the dislocation core that starts already at a temperature of 1600 K and promotes the screw dislocation core spread in {111} via the breakdown of electrostatic charge interactions. Still, further investigations under stress have to be conducted to evaluate the propensity of the screw dislocation to glide in the various slip modes of UO_2 at high-temperature.

Acknowledgements

This research is part of the EURATOM OperaHPC Project, which was co-funded by the European Union. This work was performed using HPC resources from GENCI TGCC Irène under the allocation 2022-R0131010339 and 2023-A0150906922.

References

[1] M. Oguma, Cracking and relocation behavior of nuclear fuel pellets during rise to power, Nuclear Engineering and Design 76 (1) (1983) 35–45. doi:https://doi.org/10.1016/0029-5493(83)90045-6.

[2] B. Michel, C. Nonon, J. Sercombe, F. Michel, V. Marelle, Simulation of Pellet-Cladding Interaction with the PLEIADES Fuel Performance Software Environment, Nuclear Technology 182 (2) (2013) 124–137. doi:https://doi.org/10.13182/NT13-A16424.

[3] S. Zinkle, G. Was, Materials challenges in nuclear energy, Acta Materialia 61 (3) (2013) 735–758. doi:https://doi.org/10.1016/j.actamat.2012.11.004.

[4] J. Soulacroix, B. Michel, J.-M. Gatt, R. Kubler, L. Barrallier, An aging elasto-viscoplastic model for ceramics, International Journal of Plasticity 62 (2014) 121 – 137. doi:https://doi.org/10.1016/j.ijplas.2014.07.006.

[5] D. Frazer, B. Shaffer, B. Gong, P. Peralta, J. Lian, P. Hosemann, Elevated temperature nanoindentation creep study of plastically deformed and spark plasma sintered UO_2, Journal of Nuclear Materials 545 (2021) 152605. doi:https://doi.org/10.1016/j.jnucmat.2020.152605.

[6] C. S. Yust, C. J. McHargue, Dislocation substructures in deformed uranium dioxide single crystals, Journal of nuclear materials 31 (2) (1969) 121–137. doi:https://doi.org/10.1016/0022-3115(69)90187-1.

[7] A. Alamo, J.-M. Lefebvre, J. Soullard, Deformation plastique du bioxyde d'uranium: Observation des sous-structures de dislocations, Journal of Nuclear Materials 75 (1) (1978) 145–153. doi:https://doi.org/10.1016/0022-3115(78)90038-7.

[8] P. T. Sawbridge, E. C. Sykes, Dislocation glide in UO_2 single crystals at 1600°K, Philosophical Magazine 24 (187) (1971) 33–53. doi:https://doi.org/10.1080/14786437108216422.

[9] R. J. Keller, T. E. Mitchell, A. H. Heuer, Plastic deformation in nonstoichiometric UO_{2+x} single crystals—I. deformation at low temperatures, Acta metallurgica 36 (4) (1988) 1061–1071. doi:https://doi.org/10.1016/0001-6160(88)90160-5.

[10] R. Madec, L. Portelette, B. Michel, J. Amodeo, Plastic anisotropy and composite slip: Application to uranium dioxide, Acta Materialia 255 (2023) 119016. doi:https://doi.org/10.1016/j.actamat.2023.119016.

[11] E. J. Rapperport, A. M. Huntress, Deformation Modes of Single Crystal Uranium Dioxide from 700°C to 1900°C, United States Atomic Energy Commission, Office of Technical Information (1960) 34.

[12] J. F. Byron, The yield and flow of single crystals of uranium dioxide, Journal of Nuclear Materials 28 (1) (1968) 110–114. doi:https://doi.org/10.1016/0022-3115(68)90062-7.

[13] J. S. Nadeau, Dependence of Flow Stress on Nonstoichiometry in Oxygen-Rich Uranium Dioxide at High Temperatures, Journal of the American Ceramic Society 52 (1) (1969) 1–7. doi:https://doi.org/10.1111/j.1151-2916.1968.tb11863.x-i1.

[14] M. S. Seltzer, A. H. Clauer, B. A. Wilcox, The influence of stoichiometry on compression creep of uranium dioxide single crystals, Journal of Nuclear Materials 44 (1) (1972) 43 – 56. doi:https://doi.org/10.1016/0022-3115(72)90127-4.

[15] J.-M. Lefèbvre, J. Soullard, R.-J. Gaboriaud, J. Grilhé, Calcul d'energie de fautes d'empilement dans le dioxyde d'uranium, Journal of Nuclear Materials 60 (1) (1976) 59–65. doi:https://doi.org/10.1016/0022-3115(76)90118-5.

[16] R. J. Keller, T. E. Mitchell, A. H. Heuer, Plastic deformation in nonstoichiometric UO_{2+x} single crystals—II. deformation at high temperatures, Acta metallurgica 36 (4) (1988) 1073–1083. doi:https://doi.org/10.1016/0001-6160(88)90161-7.

[17] P. Fossati, L. Van Brutzel, B. Devincre, Molecular dynamics simulation of dislocations in uranium dioxide, Journal of Nuclear Materials 443 (1) (2013) 359–365. doi:https://doi.org/10.1016/j.jnucmat.2013.07.059.

[18] L. Portelette, J. Amodeo, R. Madec, J. Soulacroix, T. Helfer, B. Michel, Crystal viscoplastic modeling of UO_2 single crystal, Journal of Nuclear Materials 510 (2018) 635–643. doi:https://doi.org/10.1016/j.jnucmat.2018.06.035.

[19] D. C. Parfitt, C. L. Bishop, M. R. Wenman, R. W. Grimes, Strain fields and line energies of dislocations in uranium dioxide., Journal of physics. Condensed matter : an Institute of Physics journal 22 (17) (2010) 175004. doi:https://doi.org/10.1088/0953-8984/22/17/175004.

[20] A. V. Lunev, A. Y. Kuksin, S. V. Starikov, Glide mobility of the 1/2[110](001) edge dislocation in UO_2 from molecular dynamics simulation, International Journal of Plasticity 89 (2017) 85 – 95. doi:https://doi.org/10.1016/j.ijplas.2016.11.004.

[21] M. Borde, M. Freyss, E. Bourasseau, B. Michel, D. Rodney, J. Amodeo, Atomic-scale modeling of 12⟨110{001} edge dislocations in uo2: Core properties and mobility, Journal of Nuclear Materials 574 (2023) 154157. doi:https://doi.org/10.1016/j.jnucmat.2022.154157.

[22] R. Skelton, A. M. Walker, Peierls-Nabarro modeling of dislocations in UO_2, Journal of Nuclear Materials 495 (2017) 202–210.

[23] L. Portelette, J. Amodeo, B. Michel, R. Madec, Athermal dislocation strengthening in UO_2, Journal of Nuclear Materials 538 (2020) 152157. doi:https://doi.org/10.1016/j.jnucmat.2020.152157.

[24] D. Terentyev, Y. N. Osetsky, D. Bacon, Effects of temperature on structure and mobility of the ⟨100⟩ edge dislocation in body-centred cubic iron, Acta Materialia 58 (7) (2010) 2477–2482. doi:https://doi.org/10.1016/j.actamat.2009.12.033.

[25] M. Poschmann, I. S. Winter, M. Asta, D. C. Chrzan, Molecular dynamics studies of $\langle a \rangle$-type screw dislocation core structure polymorphism in titanium, Phys. Rev. Mater. 6 (2022) 013603. doi:https://doi.org/10.1103/PhysRevMaterials.6.013603.

[26] A. Liu, T. Wen, J. Han, D. J. Srolovitz, Finite-temperature screw dislocation core structures and dynamics in α-titanium, npj Computational Materials 9 (1) (2023) 228. doi:https://doi.org/10.1038/s41524-023-01181-7.

[27] D. Jany, E. Rothchild, D. C. Chrzan, Polymorphic structure of $\langle a \rangle$-type screw dislocation cores in α-ti, Phys. Rev. Mater. 7 (2023) 103603. doi:10.1103/PhysRevMaterials.7.103603.

[28] S. T. Murphy, E. E. Jay, R. W. Grimes, Pipe diffusion at dislocations in UO_2, Journal of Nuclear Materials 447 (1-3) (2014) 143 – 149. doi:https://doi.org/10.1016/j.jnucmat.2013.12.029.

[29] A. V. Lunev, S. V. Starikov, T. N. Aliev, V. I. Tseplyaev, Understanding thermally-activated glide of 1/2<110>{110} screw dislocations in UO_2 – a molecular dynamics analysis, International Journal of Plasticity 110 (2018) 294 – 305. doi:https://doi.org/10.1016/j.ijplas.2018.07.003.

[30] A. Soulié, J.-P. Crocombette, A. Kraych, F. Garrido, G. Sattonnay, E. Clouet, Atomistically-informed thermal glide model for edge dislocations in uranium dioxide, Acta Materialia 150 (2018) 248–261. doi:https://doi.org/10.1016/j.actamat.2018.03.024.

[31] A. P. Thompson, H. M. Aktulga, R. Berger, D. S. Bolintineanu, W. M. Brown, P. S. Crozier, P. J. in 't Veld, A. Kohlmeyer, S. G. Moore, T. D. Nguyen, R. Shan, M. J. Stevens, J. Tranchida, C. Trott, S. J. Plimpton, LAMMPS - a flexible simulation tool for particle-based materials modeling at the atomic, meso, and continuum scales, Comp. Phys. Comm. 271 (2022) 108171. doi:https://doi.org/10.1016/j.cpc.2021.108171.

[32] M. W. D. Cooper, M. J. D. Rushton, R. W. Grimes, A many-body potential approach to modelling the thermomechanical properties of actinide oxides, Journal of Physics: Condensed Matter 26 (10) (2014) 105401. doi:https://doi.org/10.1088/0953-8984/26/10/105401.

[33] S. Potashnikov, A. Boyarchenkov, K. Nekrasov, A. Kupryazhkin, High-precision molecular dynamics simulation of UO_2–PuO_2: Pair potentials comparison in UO_2, Journal of Nuclear Materials 419 (1) (2011) 217–225. doi:https://doi.org/10.1016/j.jnucmat.2011.08.033.

[34] D. Mbongo, R. Ttot, R. Ducher, R. Dubourg, N. Salles, Improved SMTB-Q model applied to oxygen migration and pressure phase transitions in UO_2, Journal of Physics: Condensed Matter 32 (9) (2020) 095701. doi:https://doi.org/10.1088/1361-648x/ab559d.

[35] M. S. Daw, M. I. Baskes, Embedded-atom method: Derivation and application to impurities, surfaces, and other defects in metals, Phys. Rev. B 29 (1984) 6443–6453. doi:https://doi.org/10.1103/PhysRevB.29.6443.

[36] H. Balboa, L. Van Brutzel, A. Chartier, Y. Le Bouar, Assessment of empirical potential for mox nuclear fuels and thermomechanical properties, Journal of Nuclear Materials 495 (2017) 67–77. doi:https://doi.org/10.1016/j.jnucmat.2017.07.067.

[37] E. Bourasseau, C. Onofri, A. Ksibi, X. Iltis, R. C. Belin, G. Lapertot, Atomic structure of grain boundaries in UO_2 bicrystals: A coupled high resolution transmission electron microscopy/atomistic sim-

ulation approach, Scripta Materialia 206 (2022) 114191. doi:https://doi.org/10.1016/j.scriptamat.2021.114191.

[38] E. T. Dubois, J. Tranchida, J. Bouchet, J.-B. Maillet, Atomistic simulations of nuclear fuel UO_2 with machine learning interatomic potentials, Phys. Rev. Mater. 8 (2024) 025402. doi:https://doi.org/10.1103/PhysRevMaterials.8.025402.

[39] M. Borde, L. Dupuy, A. Pivano, B. Michel, D. Rodney, J. Amodeo, Interaction between 1/2<110>{110} dislocations and {110} prismatic loops in uranium dioxide: Implications for strain-hardening under irradiation, International Journal of Plasticity 168 (2023) 103702. doi:https://doi.org/10.1016/j.ijplas.2023.103702.

[40] S. W. Rick, S. J. Stuart, B. J. Berne, Dynamical Fluctuating Charge Force Fields: Application to Liquid Water, The journal of chemical physics 7 (101) (1994) 6141–6156. doi:https://doi.org/10.48550/arxiv.chem-ph/9406002.

[41] N. Salles, O. Politano, E. Amzallag, R. Tétot, Molecular dynamics study of high-pressure alumina polymorphs with a tight-binding variable-charge model, Computational Materials Science 111 (2016) 181–189. doi:https://doi.org/10.1016/j.commatsci.2015.09.017.

[42] Q. Xu, N. Salles, J. Chevalier, J. Amodeo, Atomistic simulation and interatomic potential comparison in α-Al_2O_3 : lattice, surface and extended-defects properties, Modelling and Simulation in Materials Science and Engineering 30 (3) (2022) 035008. doi:https://doi.org/10.1088/1361-651x/ac4d76.

[43] R. W. Hockney, J. W. Eastwood, Computer simulation using particles, crc Press, 1989.

[44] D. Wolf, P. Keblinski, S. R. Phillpot, J. Eggebrecht, Exact method for the simulation of Coulombic systems by spherically truncated, pairwise r[sup 1] summation, The Journal of Chemical Physics 110 (17) (1999) 8254. doi:10.1063/1.478738.

[45] P. Hirel, Atomsk: A tool for manipulating and converting atomic data files, Computer Physics Communications 197 (2015) 212–219. doi:https://doi.org/10.1016/j.cpc.2015.07.012.

[46] D. Rodney, L. Ventelon, E. Clouet, L. Pizzagalli, F. Willaime, Ab initio modeling of dislocation core properties in metals and semiconductors, Acta Materialia 124 (2017) 633–659. doi:https://doi.org/10.1016/j.actamat.2016.09.049.

[47] W. Cai, V. V. Bulatov, J. Chang, J. Li, S. Yip, Periodic image effects in dislocation modelling, Philosophical Magazine 83 (5) (2003) 539–567. doi:https://doi.org/10.1080/0141861021000051109.

[48] E. Clouet, Ab Initio Models of Dislocations, Springer International Publishing, Cham, 2018, pp. 1–22. doi:https://doi.org/10.1007/978-3-319-42913-7_22-1.

[49] E. Bitzek, P. Koskinen, F. Gähler, M. Moseler, P. Gumbsch, Structural relaxation made simple, Phys. Rev. Lett. 97 (2006) 170201. doi:https://doi.org/10.1103/PhysRevLett.97.170201.

[50] E. Clouet, Babel software.
URL http://emmanuel.clouet.free.fr/Programs/Babel/index.html

[51] P. M. Larsen, S. Schmidt, J. Schiøtz, Robust structural identification via polyhedral template matching, Modelling and Simulation in Materials Science and Engineering 24 (5) (2016) 055007, publisher: IOP Publishing. doi:https://doi.org/10.1088/0965-0393/24/5/055007.

[52] A. Stukowski, Visualization and analysis of atomistic simulation data with ovito–the open visualization tool, Modelling and Simulation in Materials Science and Engineering 18 (1) (2009) 015012. doi:https://doi.org/10.1088/0965-0393/18/1/015012.

[53] L. Hale, Atomman: the atomistic manipulation toolkit.
URL https://www.ctcms.nist.gov/potentials/atomman/

[54] A. Aslanides, V. Pontikis, Atomistic study of dislocation cores in aluminium and copper, Computational Materials Science 10 (1) (1998) 401–405, computational Modelling of Issues in Materials Science. doi:https://doi.org/10.1016/S0927-0256(97)00109-2.

[55] D. Rodney, G. Martin, Dislocation pinning by small interstitial loops: A molecular dynamics study, Phys. Rev. Lett. 82 (1999) 3272–3275. doi:https://doi.org/10.1103/PhysRevLett.82.3272.

[56] Y. N. Osetsky, D. J. Bacon, An atomic-level model for studying the dynamics of edge dislocations in metals, Modelling and Simulation in Materials Science and Engineering 11 (4) (2003) 427. doi:https://doi.org/10.1088/0965-0393/11/4/302.

[57] S. Nosé, A molecular dynamics method for simulations in the canonical ensemble, Molecular Physics 52 (2) (1984) 255–268. doi:https://doi.org/10.1080/00268978400101201.

[58] V. V. B. Wei Cai, Computer simulations of dislocations, Vol. 3, OUP Oxford, 2006.

[59] C. Onofri, J. Monchoux, J. Amodeo, R. Madec, C. Sabathier, H. Palancher, J. Fouet, D. Drouan, M. Legros, Versatility of dislocation motions in polycrystalline UO_2 deformed at 1550°C investigated by TEM, Scripta Materialia 244 (2024) 116034. doi:https://doi.org/10.1016/j.scriptamat.2024.116034.

[60] J. Hiernaut, G. J. Hyland, C. Ronchi, Premelting transition in uranium dioxide, International Journal of Thermophysics 14 (1993) 259–283.

[61] C. Ronchi, G. Hyland, Analysis of recent measurements of the heat capacity of uranium dioxide, Journal of Alloys and Compounds 213-214 (1994) 159–168, international Conference on Actinides. doi:https://doi.org/10.1016/0925-8388(94)90897-4.

[62] T. Pavlov, M. Wenman, L. Vlahovic, D. Robba, R. Konings, P. Van Uffelen, R. Grimes, Measurement and interpretation of the thermophysical properties of UO_2 at high temperatures: The viral effect of oxygen defects, Acta Materialia 139 (2017) 138–154. doi:https://doi.org/10.1016/j.actamat.2017.07.060.

[63] V. M. Carr, A. V. Chadwick, R. Saghafian, The electrical conductivity of PbF_2 and $SrCl_2$ crystals at high temperatures, Journal of Physics C: Solid State Physics 11 (15) (1978) L637. doi:https://doi.org/10.1088/0022-3719/11/15/006.

[64] J. P. Goff, W. Hayes, S. Hull, M. T. Hutchings, Neutron powder diffusion study of the fast-ion transition and specific heat anomaly in beta -lead fluoride, Journal of Physics: Condensed Matter 3 (21) (1991) 3677. doi:https://doi.org/10.1088/0953-8984/3/21/001.

[65] S. Hull, S. T. Norberg, I. Ahmed, S. G. Eriksson, C. E. Mohn, High temperature crystal structures and superionic properties of $SrCl_2$, $SrBr_2$ and $BaBr_2$, Journal of Solid State Chemistry 184 (11) (2011) 2925–2935. doi:https://doi.org/10.1016/j.jssc.2011.09.004.

[66] D. Bathellier, M. Lainet, M. Freyss, P. Olsson, E. Bourasseau, A new heat capacity law for UO_2, PuO_2 and (U,Pu)O_2 derived from molecular dynamics simulations and useable in fuel performance codes, Journal of Nuclear Materials 549 (2021) 152877. doi:https://doi.org/10.1016/j.jnucmat.2021.152877.

[67] A. V. Lunev, B. A. Tarasov, A classical molecular dynamics study of the correlation between the bredig transition and thermal conductivity of stoichiometric uranium dioxide, Journal of Nuclear Materials 415 (2) (2011) 217–221. doi:https://doi.org/10.1016/j.jnucmat.2011.06.009.

[68] S. Starikov, M. Korneva, Description of phase transitions through accumulation of point defects: UN, UO_2 and UC, Journal of Nuclear Materials 510 (2018) 373–381. doi:10.1016/j.jnucmat.2018.08.025.

[69] P. C. M. Fossati, P. A. Burr, M. W. D. Cooper, C. O. T. Galvin, R. W. Grimes, Superionic transition in uranium dioxide: Insights from molecular dynamics and lattice dynamics simulations, Physical Review Materials 8 (11) (2024) 115404. doi:10.1103/physrevmaterials.8.115404.